ISBN: 978-3-95450-262-2 ISSN: 2673-5350 doi: 10.18429/JACoW-IBIC2025-TUDC01

STUDY OF SUPER-RESOLUTION RECONSTRUCTION IN TRANSVERSE PHASE SPACE MEASURED VIA SLIT-SCANNING METHOD

H. Hu*, B. Zhou*, Y. Xia, D. Lu, Y. Zeng, Y. Wang, K. Liu, T. Hu†
Huazhong University of Science and Technology, Wuhan, China

Abstract

Electron beam injectors, critical to advanced light sources and ultrafast diffraction systems, require precise transverse phase space diagnostics to optimize beam quality. Conventional slit-scanning combined with computed tomography (CT) enables non-presumptive phase space reconstruction but faces resolution limitations under sparse sampling. This study introduces a deep learning framework to achieve super-resolution reconstruction from minimal scan data. By integrating beam transport physics with neural networks, the method overcomes resolution degradation in low-data regimes. The proposed algorithm, coupled with beam dynamics simulations, forms a systematic engineering solution for high-fidelity diagnostics. This approach enhances phase space characterization efficiency, supporting accelerator commissioning with reduced experimental overhead.

INTRODUCTION

Accurate transverse phase space diagnostics are essential for optimizing beam quality in electron beam injectors, which are critical components of advanced light sources and ultrafast electron diffraction systems. The slit-scanning method combined with computed tomography [1,2] (CT) enables non-presumptive phase space reconstruction, allowing full distribution characterization without assuming a prior beam model. However, achieving high resolution requires dense angular sampling, which increases measurement time and demands high mechanical and beam stability.

In practical commissioning and tuning, constraints on beam time and stability often force operation in sparse sampling regimes, leading to severe resolution degradation in conventional algebraic reconstruction techniques. This limits the ability to resolve fine phase space features and accurately determine beam parameters such as emittance, thus impacting both diagnostic reliability and accelerator optimization efficiency.

To overcome these limitations, we propose a physics-informed deep learning framework [3] for super-resolution [4] phase space reconstruction from minimal slit-scan data. Trained on synthetic datasets from beam dynamics simulations, the network learns to recover high-frequency details lost in undersampled measurements while ensuring physical consistency. Numerical studies on a low-energy injector test platform demonstrate significant resolution gains and robustness over traditional methods, offering a promising approach for efficient, high-fidelity beam diagnostics.

* equal contribution
† TongningHu@hust.edu.cn

PRINCIPLE OF SLIT-SCANNING PHASE SPACE MEASUREMENT

Principle

As defined in Eq. (1), the transverse geometric emittance characterizes the phase space area of an electron bunch. However, in practical measurements the particle angles cannot be directly accessed. Instead, the slit-scanning method is commonly employed as an indirect diagnostic of beam emittance [5].

$$\varepsilon \equiv \sqrt{\langle x^2\rangle\langle x'^2\rangle - \langle xx'\rangle^2}. \tag{1}$$

The principle of this method is illustrated in Fig. 1. A typical slit-scan system consists of a transversely movable slit, a downstream fluorescent screen, and a drift section in between. By sampling the beam with a sufficiently narrow slit, a fraction of the bunch is transmitted through and subsequently drifts to the screen. The transverse position of the transmitted beamlet on the screen, together with the drift length, allows the reconstruction of its divergence angle. Repeating this process while incrementally shifting the slit provides a series of beamlets with measured positions and divergences [6]. From these scanning data, the transverse geometric emittance of the main bunch can be approximated. The statistic in Eq. (1) can be derived from Eqs. (2)-(4) [7].

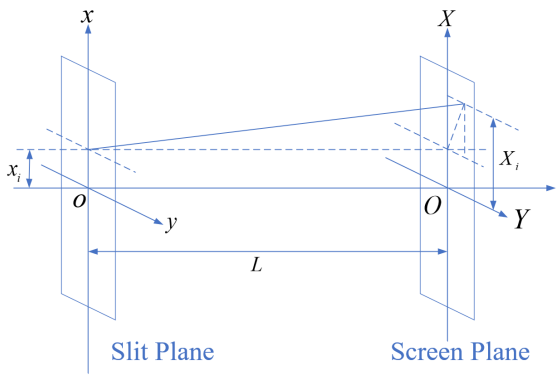

Figure 1: Principle of Slit-Scanning phase space measurement.

$$\langle x^2\rangle = \frac{1}{N}\sum_{i=1}^{N}(x_i - \bar{x})^2 \approx \frac{1}{N}\sum_{j=1}^{p} n_j (x_{sj} - \bar{x})^2, \tag{2}$$

$$\left\langle x'^2\right\rangle = \frac{1}{N}\sum_{i=1}^{N}(x'_i - \bar{x'})^2 \tag{3}$$

ISBN: 978-3-95450-262-2 ISSN: 2673-5350 doi: 10.18429/JACoW-IBIC2025-TUDC01

$$\approx \frac{1}{N}\sum_{j=1}^{p}\left[n_j\sigma_{x'j}^2 + n_j\left(\bar{x_j'} - \bar{x'}\right)^2\right],$$

$$\langle xx'\rangle = \frac{1}{N}\sum_{i=1}^{N}(x_i - \bar{x})(x_i' - \bar{x'}) \quad (4)$$

$$\approx \frac{1}{N}\sum_{j=1}^{p}\left(n_j x_{sj}\bar{x_j'} - N\bar{x}\bar{x'}\right),$$

where: p is the number of slits;
x_{sj} is the j-th slit position;
n_j is number of particles through the j-th slit;
$\bar{x}$ is the mean position of all particles;
$\bar{X_j} = \frac{1}{n_j}\sum_{i=1}^{n_j} X_{ji}$ is the mean position of the j-th spots on screen;
$\bar{x_j'} = (\bar{X_j} - x_{sj})/L$, is the mean divergence of particles passing through the j-th slit;
$\bar{x'} = \frac{1}{N}\sum_{j=1}^{p} n_j\bar{x'}_j$ is the mean divergence angle of all beamlets;
$\sigma_{x_j'} = (\sqrt{\frac{1}{n_j}\sum_{i=1}^{n_j}\left(X_{ji} - \bar{X_j}\right)^2})/L$, is the rms divergence of beamlet at the j-th slit.

Virtual Test

Based on the general beam diagnostic platform constructed at Huazhong University of Science and Technology [8], a virtual test of emittance measurement using the slit-scan method was carried out. The parameters of the test beam and the slit-scan system are listed in Table 1. The test beam distributions were obtained from upstream electron gun simulations, while the system parameters were taken from the actual design and fabrication of the diagnostic device.

Table 1: Initial Beam and Slit Scanning Parameters

Main Parameters	Set Values
Total number of particles N	20000
Kinetic energy E_k	10 MeV
Real emittances ε	0.4867 μm.rad
Distance from gun to slit l	1.930 m
Distance from slit to screen L	1.369 m
Width of the slits Δx	0.2 mm
Number of slits n	13

The measured phase space is illustrated in Fig. 2. Figures 2(a) and (b) show the transverse beam profile at the slit position and the corresponding phase space, both derived from beam dynamics simulations. Figure 2(c) simulates the image recorded by the CCD camera on the downstream fluorescent screen, and Fig. 2(d) presents the reconstructed phase space obtained from slit sampling. By projecting the image in Fig. 2(c) and applying Gaussian fitting, the fitted parameters can be substituted into Eqs. (1)-(4) to calculate the emittance of the original bunch.

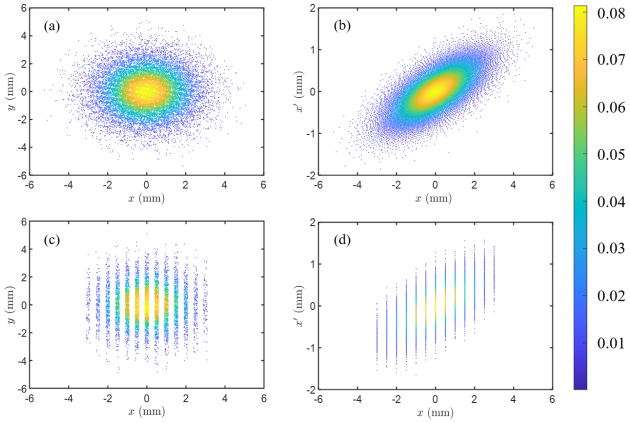

Figure 2: Beam spots and phase spaces before slit and after slit sampling

DEEP LEARNING-BASED SUPER-RESOLUTION FRAMEWORK

Training Dataset Preparation

The training dataset was generated using the ASTRA beam dynamics simulation, which provided simulated electron bunch phase space distributions under randomized beam conditions. Within predefined parameter ranges shown in Table 2, the transverse emittance, beam size, and divergence were varied to cover a broad spectrum of realistic injector scenarios. For each generated distribution, the slit-scanning process described in Section II was numerically simulated to produce corresponding low-resolution measurements. In this dataset, domain A contains undersampled transverse phase space images of size 512 × 512 obtained from the simulated slit-scan, while domain B consists of the complete high-resolution phase space distributions of size 1024×1024. A total of 4000 image pairs were generated, with one-to-one correspondence between domains A and B. The objective of the proposed framework is to learn the mapping from A to B, effectively reconstructing high-fidelity phase space from minimal sampling data. Representative examples from the training set, covering various beam sizes, divergences, and projection angles, are illustrated in Fig. 3.

Table 2: Initial Beam Parameter Ranges for Generating Beam Distribution Dataset

Parameter	Value Range	Unit
RMS beam size	[1,12]	mm
Correlated divergence	[-0.1,0.1]	mrad
Geometric emittance	[1,10]	mm·mrad

Network Architecture

The proposed framework employs a CycleGAN-based [9] architecture shown as Fig. 4 tailored for transverse phase space super-resolution. Two ResNet-based generators,

ISBN: 978-3-95450-262-2 ISSN: 2673-5350 doi: 10.18429/JACoW-IBIC2025-TUDC01

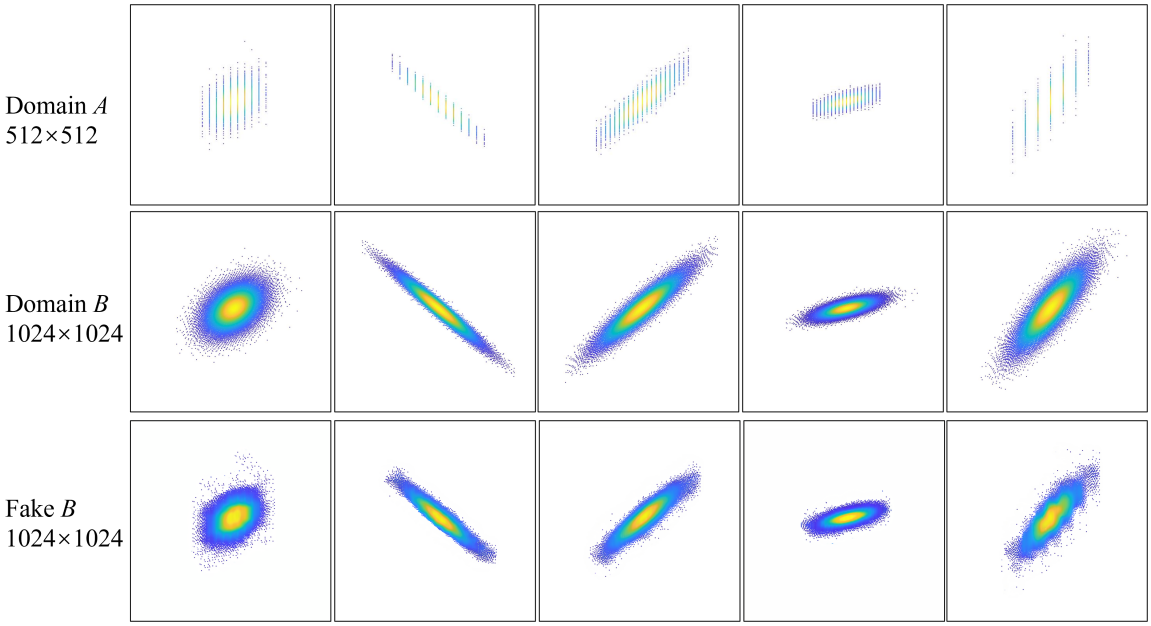

Figure 3: Results of phase space reconstruction. Top row: low-resolution slit-scan images (512×512). Middle row: ground truth high-resolution phase space distributions (1024×1024) from beam simulations. Bottom row: reconstructed high-resolution images (1024×1024) generated by the proposed CycleGAN framework.

$G_{A\to B}$ and $G_{B\to A}$, learn bidirectional mappings between low-resolution (A) and high-resolution (B) phase space domains. Each generator adopts a ResNet-9blocks design, consisting of an initial 7×7 convolutional layer with reflection padding, two strided downsampling stages, nine residual blocks to capture nonlinear transformations, and symmetric transposed-convolution upsampling layers. Instance normalization and ReLU activations are applied throughout to ensure stable training. Two PatchGAN discriminators, D_B and D_A [10], operate on local patches of the phase space to encourage fine-scale realism in the reconstructed distributions.

Loss Function

In this work, A denotes the low-resolution (LR) transverse phase space reconstructed from sparse slit-scan data, while B represents the high-resolution (HR) reference distribution obtained from dense sampling or high-fidelity simulations. The generators $G_{A\to B}$ and $G_{B\to A}$ are trained to translate between these domains while preserving the essential physics of the beam.

The training objective integrates three complementary mechanisms:

1. **Adversarial loss** ensures that the generated HR distribution $G_{A\to B}(A)$ is statistically indistinguishable from true HR data, effectively matching the underlying probability density of the beam distribution.

2. **Cycle-consistency loss** enforces $A\to B\to A$ and $B\to A\to B$ mappings to recover the original distribution, thereby preserving physical beam quantities such as normalized emittance and Twiss parameters.

3. **Identity loss** constrains the generators to behave as near-identity mappings when the input already belongs to the target resolution domain, preventing unnecessary distortions and maintaining genuine beam features.

The total generator loss is defined as:

$$\begin{aligned} L_G = {} & L_{GAN}(G_{A\to B}, D_B) + L_{GAN}(G_{B\to A}, D_A) \\ & + \lambda_A L_{cyc}(G_{B\to A}(G_{A\to B}(A)), A) \\ & + \lambda_B L_{cyc}(G_{A\to B}(G_{B\to A}(B)), B) \\ & + \lambda_{idt} L_{idt}, \end{aligned} \tag{5}$$

where λ_A, λ_B, and λ_{idt} control the relative contributions of the cycle and identity terms. This formulation not only drives the network to recover fine-scale phase space structures lost in undersampled measurements but also enforces beam dynamics constraints, ensuring coherence, statistical consistency, and geometric fidelity of the reconstructed phase space.

Results

Figure 3 presents representative examples of transverse phase space reconstruction using the proposed CycleGAN-based framework. The first row shows the low-resolution slit-scan images (512×512 pixels), which are obtained from simulated slit sampling as described in Section "Principle of Slit-Scanning Phase Space Measurement". Due to the sparse sampling process, these images exhibit pronounced strip-like artifacts and lack fine structural details of the beam distribution.

The second row displays the corresponding ground truth high-resolution phase space distributions (1024×1024 pixels) generated directly from beam dynamics simulations.

ISBN: 978-3-95450-262-2 ISSN: 2673-5350 doi: 10.18429/JACoW-IBIC2025-TUDC01

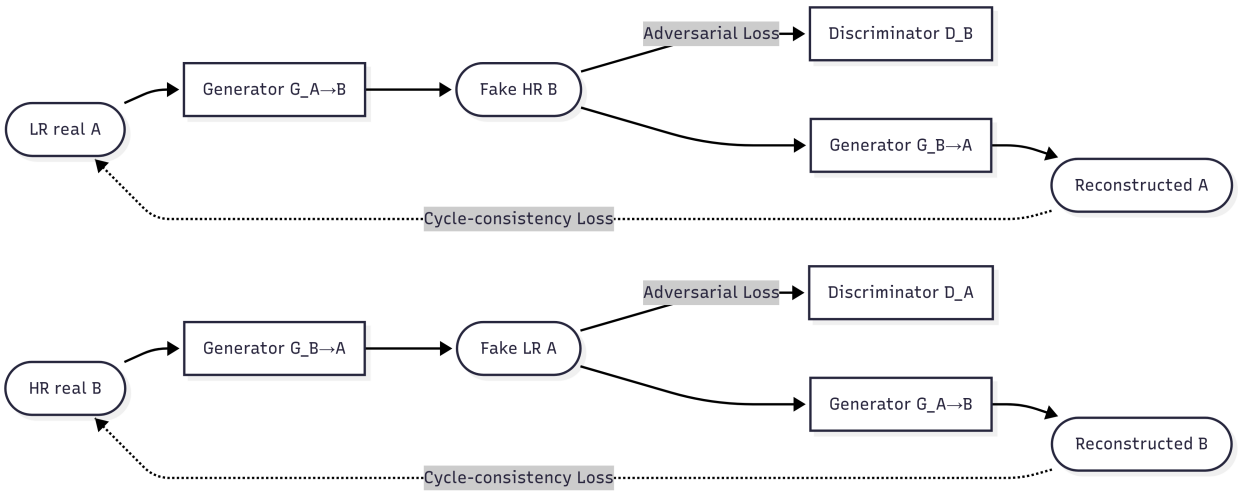

Figure 4: CycleGAN-based super-resolution model for transverse phase space. The framework includes adversarial loss, cycle-consistency loss, and identity loss to ensure both high-fidelity reconstruction and physical consistency.

These images capture the intrinsic transverse beam features with full resolution, serving as the target domain in the training dataset.

The third row shows the reconstructed high-resolution images ($\hat{B}$) generated by $G_{A\to B}$ of the CycleGAN framework. By learning the mapping between domain A (slit-scan data) and domain B (ground truth distributions), the network is able to recover high-frequency details and reproduce smooth phase space contours from undersampled inputs. The reconstruction quality improves as the number of slit samplings increases, while limited sampling leads to distortions, as seen in the rightmost case where only seven slit positions are used. Another limitation arises at the beam edges: since the slit-scan method cannot effectively capture particles in sparsely populated outer regions, the corresponding features are underrepresented in domain A, and the network struggles to recover them in $\hat{B}$. This effect is more pronounced for beams with large emittance. Nevertheless, for the purpose of beam parameter evaluation, such as emittance fitting, the influence of edge particles is relatively minor compared to the dense beam core. Overall, the reconstructed results demonstrate good agreement with the true phase space distributions and confirm the capability of the proposed method to mitigate resolution loss in sparse sampling regimes.

CONCLUSION

In this work, a CycleGAN-based deep learning framework was developed to achieve super-resolution reconstruction of transverse phase space measured via the slit-scanning method. By combining beam dynamics simulations with adversarial training, the model successfully learned the mapping between undersampled slit-scan images and corresponding high-resolution phase space distributions.

Numerical studies demonstrate that the proposed method can recover fine structural details and smooth contours from sparse measurements, substantially improving reconstruction fidelity compared with conventional algebraic techniques. The performance improves with the number of slit samplings, whereas limited sampling (e.g. only seven slit positions) leads to visible distortions and increased errors. In addition, the reconstruction of edge regions remains less accurate due to the intrinsic limitation of the slit-scan method, which underrepresents sparsely populated beam halo particles. This effect is more pronounced for beams with large emittance. Nevertheless, since beam parameter evaluation such as emittance fitting is dominated by the dense beam core, the impact of edge reconstruction errors is relatively minor.

Overall, the proposed framework provides an efficient and systematic tool for high-fidelity phase space diagnostics, reducing experimental overhead in injector commissioning. Future work will focus on experimental validation, improving robustness against measurement noise, and extending the method to other diagnostic modalities in accelerator physics.

ACKNOWLEDGEMENTS

This work was supported by the National Key R & D Program of China (No.2024YFA1612200) and the National Natural Science Foundation of China (No.12341501).

REFERENCES

[1] A. Wolski, D. Botelho, D. Dunning, and A. E. Pollard, "Accelerator beam phase space tomography using machine learning to account for variations in beamline components", *J. Instrum.*, vol. 19, no. 07, p. P07013, 2024. doi:10.1088/1748-0221/19/07/P07013

[2] A. Wolski, M. A. Johnson, M. King, B. L. Militsyn, and P. H. Williams, "Transverse phase space tomography in an accelerator test facility using image compression and machine learning", *Phys. Rev. Accel. Beams*, vol. 25, no. 12, p. 122 803, 2022. doi:10.1103/PhysRevAccelBeams.25.122803

ISBN: 978-3-95450-262-2 ISSN: 2673-5350 doi: 10.18429/JACoW-IBIC2025-TUDC01

[3] R. Roussel *et al.*, "Efficient six-dimensional phase space reconstructions from experimental measurements using generative machine learning", *Phys. Rev. Accel. Beams*, vol. 27, no. 9, p. 094 601, 2024. doi:10.1103/PhysRevAccelBeams.27.094601

[4] C. Ledig *et al.*, "Photo-realistic single image super-resolution using a generative adversarial network", in *2017 IEEE Conference on Computer Vision and Pattern Recognition (CVPR)*, HI, USA, pp. 105–114, 2017. doi:10.1109/CVPR.2017.19

[5] S. G. Anderson, J. B. Rosenzweig, G. P. LeSage, and J. K. Crane, "Space-charge effects in high brightness electron beam emittance measurements", *Phys. Rev. Spec. Top. Accel. Beams*, vol. 5, no. 1, p. 014 201, 2002. doi:10.1103/PhysRevSTAB.5.014201

[6] P. Forck, "Lecture notes on beam instrumentation and diagnostics", in *Proceedings of the Joint University Accelerator School (JUAS 2010)*, 2011. https://www-bd.gsi.de/conf/juas/juas_script.pdf

[7] M. Zhang, "Emittance formula for slits and pepper pot measurement", Fermi National Accelerator Laboratory (FNAL), Batavia, IL, United States, Tech. Rep. FERMILAB-TM-1988, 1996. doi:10.2172/395453

[8] T. N. Hu, Y. F. Zeng, and K. F. Liu, "Design considerations of a magnet-based diagnosis system with compact layout for typical beam injector", *IEEE Trans. Appl. Supercond.*, vol. 34, no. 5, pp. 1–5, 2024. doi:10.1109/TASC.2024.3355359

[9] J.-Y. Zhu, T. Park, P. Isola, and A. A. Efros, "Unpaired image-to-image translation using cycle-consistent adversarial networks", in *IEEE International Conference on Computer Vision (ICCV 2017)*, UC Berkeley, USA, 2017.

[10] P. Isola, J.-Y. Zhu, T. Zhou, and A. A. Efros, "Image-to-image translation with conditional adversarial networks", in *2017 IEEE Conference on Computer Vision and Pattern Recognition (CVPR)*, HI, USA, pp. 5967–5976, 2017. doi:10.1109/CVPR.2017.632